Benchmarking a modified version of the CIV3 nonrelativistic atomic-structure code within Na-like-tungsten *R*-matrix calculations

M. D. Turkington, C. P. Ballance, A. Hibbert, and C. A. Ramsbottom
School of Mathematics and Physics, Queen's University Belfast, Belfast BT7 1NN, Northern Ireland, United Kingdom
(Received 28 April 2016; published 17 August 2016)

In this work we explore the validity of employing a modified version of the nonrelativistic structure code CIV3 for heavy, highly charged systems, using Na-like tungsten as a simple benchmark. Consequently, we present radiative and subsequent collisional atomic data compared with corresponding results from a fully relativistic structure and collisional model. Our motivation for this line of study is to benchmark CIV3 against the relativistic GRASP^0 structure code. This is an important study as CIV3 wave functions in nonrelativistic *R*-matrix calculations are computationally less expensive than their Dirac counterparts. There are very few existing data for the W LXIV ion in the literature with which we can compare except for an incomplete set of energy levels available from the NIST database. The overall accuracy of the present results is thus determined by the comparison between the CIV3 and GRASP^0 structure codes alongside collisional atomic data computed by the *R*-matrix Breit-Pauli and Dirac codes. It is found that the electron-impact collision strengths and effective collision strengths computed by these differing methods are in good general agreement for the majority of the transitions considered, across a broad range of electron temperatures.

DOI: 10.1103/PhysRevA.94.022508

I. INTRODUCTION

The ITER tokamak is a defining landmark on the road to the world's first commercial fusion reactor. The choice of material to be used in the plasma facing components of the diverter region of the reactor was a difficult one, as there are only a few elements that can withstand temperatures of 20–30 keV, consistent with the operating parameters of ITER. It is now certain that the reactor will use tungsten as the plasma facing material [1], owing to its high melting point and thermal conductivity and low sputtering rate. Regardless, tungsten from the plasma facing components of the tokamak will enter the plasma in various ion stages and this impurity must be characterized. The presence of such impurities has the effect of increasing power losses by producing line emission in the x-ray and EUV regions. Thus, atomic data concerning all stages of tungsten ionization are necessary for diagnostic applications. To this end, the paucity of radiative and collisional data has been urgently addressed in the past decade in works by Ballance *et al.* [2], Safronova *et al.* [3], and Aggarwal *et al.* [4].

In this work we calculate energy levels, transition rates, collision strengths, and Maxwellian averaged effective collision strengths for the W LXIV ion. Due to the presence of only one valence electron, we are able to consider all hydrogeniclike levels up to the $2p^6 5g\ ^2G$ configuration, while including only 21 fine-structure levels. Hence it is not computationally expensive to calculate and retain radiative and collisional data for all transitions between these levels.

To date there have been very few publications concerning the W LXIV ion. The largest theoretical calculation we are aware of was carried out by Kramida and Shirai [5] and computed theoretical energy levels up to the $2p^6 5g\ ^2G$ configuration. In addition, Dipti *et al.* [6] presented energy levels and radiative data for transitions from the $2p^6 3s\ ^2S_{1/2}$ ground state to several $2p^5 3l3l'$ configurations, using observations from an electron-beam ion trap source and from calculations adopting relativistic distorted-wave theory.

The calculations presented here were carried out using two different methods. Initially the configuration-interaction CIV3 code [7,8] was utilized, incorporating the Breit-Pauli approximation to the relativistic Hamiltonian. In a second evaluation the fully relativistic GRASP^0 code [9–11] was adopted. The reason for using these two separate structure codes was twofold. First and foremost, we wished to see if the wave functions derived from the nonrelativistic orbital parameters computed in the CIV3 code, which was designed for calculations involving lowly ionized intermediate-Z ions, could produce accurate structural atomic data for the heavy, highly ionized W LXIV ion. In both evaluations, we included the $2p^6 nl$ ($n = 3,4,5$ and $l = s,p,d,f,g$) configurations, which led to a total of 210 individual forbidden and allowed transitions. A benefit of being able to obtain precise atomic data from CIV3 is that the orbital parameters can be incorporated in the *R*-matrix transformation methods ICFT [12] and RMATRXII [13]. These codes require substantially fewer computational facilities than the fully relativistic DARC suite, a desirable feature because all ionization stages of the tungsten are required for ITER plasma diagnostics, constituting a considerable effort. Second, due to the sparsity of experimental or theoretical data for this ion, we decided that having two sets of data with which to compare would help to discern the validity of our calculations.

The remainder of the paper is as follows. In Sec. II we present a summary of the relevant configuration-interaction theory employed. Tabulations of energy levels and transition rates are presented and comparisons are made between the results from the CIV3 and GRASP^0 codes. Section III outlines the basic collisional Breit-Pauli and Dirac *R*-matrix theories. We present the collision strengths and Maxwellian averaged effective collision strengths for a selection of allowed and forbidden transitions over a wide range of electron temperatures of importance. In Sec. IV we derive photon emissivity coefficients ($\mathcal{PEC}$s) for the 20 strongest transitions in our model. Finally, in Sec. V we draw conclusions about the viability of the employed methods and the accuracy of the atomic data produced and discuss the goals of future research.

II. STRUCTURE CALCULATIONS

A. CIV3 calculations

In the configuration-interaction method the total wave function describing the target ion is expressed as the sum of a set of configuration-state functions (CSFs) $\Phi_i(\alpha_i \pi)$,

$$\Psi(J\pi) = \sum_i^M a_i \Phi_i(\alpha_i J\pi), \tag{1}$$

where the $\{a_i\}$ are the configuration-interaction (CI) expansion coefficients and α_i denotes the angular momentum coupling scheme used. For a specific set of CSFs, the expansion coefficients are the components of the eigenvectors of the Hamiltonian matrix with elements $\langle \Phi_i | H | \Phi_j \rangle$. The CSFs are constructed from one-electron orbitals, composed of radial, angular, and spin components. In CIV3 each radial function is represented as a linear combination of normalized Slater-type orbitals

$$P_{nl}(r) = \sum_{j=1}^{k} c_{jnl} \left[\frac{(2\zeta_{jnl})^{2I_{jnl}+1}}{(2I_{jnl})!} \right] r^{I_{jnl}} \exp(-\zeta_{jnl} r). \tag{2}$$

An orthonormality condition is imposed on the radial functions such that

$$\int_0^\infty P_{nl}(r) P_{n'l}(r) dr = \delta_{nn'}. \tag{3}$$

If the energy eigenvalues E_i of the Hamiltonian matrix are ordered such that $E_i < E_{i+1}$, then

$$E_i > E_i^{\text{exact}}, \tag{4}$$

where the exact energy eigenvalue corresponds to that of the coupling scheme adopted [14]. These form variational principles from which the radial functions may be optimized. During a typical optimization, we keep the powers of the radial distance I_{jnl} fixed and allow the exponents ζ_{jnl} and the coefficients c_{jnl} to vary freely, subject to (3). For a highly ionized heavy system such as the W LXIV ion, relativistic effects play a crucial role. CIV3 accounts for such effects by supplementing the nonrelativistic Schrödinger Hamiltonian with relativistic Breit-Pauli terms; the spin-independent Darwin and mass-correction terms; and the spin-dependent spin-orbit, spin-other-orbit, and spin-spin interactions.

B. Radial function parameters

We outline in Table I the optimization procedures adopted in the present CIV3 evaluation for the 15 spectroscopic orbitals included in the representation of the wave-function expansions of the target ion. The radial parameters for the $1s$ core orbital were chosen to be the Hartree-Fock values for the $5d^4 6s\ ^6D$ ground state of the W II given by McLean and McLean [15]. The parameters for the remaining orbitals were obtained in the following manner. For $2s$ and $2p$ we initially chose the Hartree-Fock values of the ground state of the W II given in [15], but these were then reoptimized. The optimal $1s$ orbital is largely unchanged as the number of electrons in the outer shell varies, so we did not reoptimize the $1s$ radial function for this 11-electron ion from that of the 73-electron ion. The parameters for $2s$, along with $3d$, were optimized on the energy of the $2p^6 3d\ ^2D$ state, while for $2p$, along with $3s$, we optimized on the energy of the $2p^6 3s\ ^2S$ state. The remaining orbitals nl were optimized on the energy of the $2p^6 nl$ state, in some cases (for $l > 0$) with the mass-correction operator included so as to capture the relativistic contraction of these outer orbitals. Additionally, we made further small adjustments to some of the radial function exponents in order to improve the fine-structure splitting between the states. The radial parameters (c_{jnl}, I_{jnl}, and ζ_{jnl}) for all the orbitals are tabulated in Table II.

TABLE I. Optimization of the orbital parameters.

Orbital	Optimized on energy of	
$1s$	HF from $5d^4 6s\ ^6D$ ground state of W II	
$2s$, $3d$	$2p^6 3d\ ^2D$	
$2p$, $3s$	$2p^6 3s\ ^2S$	
$4s$	$2p^6 4s\ ^2S$	
$5s$	$2p^6 5s\ ^2S$	
$3p$	$2p^6 3p\ ^2P^o$	
$4p$	$2p^6 4p\ ^2P^o$	(+mass correction)
$5p$	$2p^6 5p\ ^2P^o$	(+mass correction)
$4d$	$2p^6 4d\ ^2D$	(+mass correction)
$5d$	$2p^6 5d\ ^2D$	(+mass correction)
$4f$	$2p^6 4f\ ^2F^o$	
$5f$	$2p^6 5f\ ^2F^o$	(+mass correction)
$5g$	$2p^6 5g\ ^2G$	(+mass correction)

C. Determination of orbitals using GRASP^0

GRASP^0 is a relativistic atomic structure package used to generate relativistic orbitals within the multiconfiguration Dirac-Fock approximation. In particular, the 25 relativistic orbitals employed in our model were obtained from a Dirac-Coulomb Hamiltonian of the form

$$H_D = \sum_i \left(c\boldsymbol{\alpha} \cdot \boldsymbol{p}_i + (\boldsymbol{\beta} - 1)c^2 - \frac{Z}{r_i} \right) + \sum_{i>j=1} \frac{1}{r_{ij}}. \tag{5}$$

Here the electrons are labeled i and j, $\boldsymbol{\alpha}$ and $\boldsymbol{\beta}$ are matrices associated with the Pauli spin matrices, $\boldsymbol{p}_i$ is the electron momentum operator, c is the speed of light, and Z is the atomic number. Unlike the orbitals derived using CIV3, these relativistic orbitals are formed from a large component $\mathcal{P}_{nl}$ and small component $\mathcal{Q}_{nl}$. The orbitals were not optimized on any subset of levels, but on the average of the best minimization of all levels. The GRASP^0 values are used as the benchmark by which CIV3 is compared.

D. Radiative atomic data

We list in Table III the energy levels in rydbergs for the lowest 21 fine-structure terms, relative to the $2p^6 3s\ ^2S$ ground state of W LXIV, evaluated in the present 12-configuration model. Comparisons are made between energies derived from the orbitals in CIV3 as discussed in the previous subsection, those from the orbitals determined using the fully relativistic GRASP^0 package and the separations available in the NIST database [5]. Considering the fully relativistic GRASP^0 energies first, we see that there is quite good agreement with NIST for all fine-structure levels. Since this is a structure code

TABLE II. Radial parameters for the W LXIV used in the CIV3 calculation.

nl	$\langle r \rangle$	c_{jnl}	I_{jnl}	ζ_{jnl}	nl	$\langle r \rangle$	c_{jnl}	I_{jnl}	ζ_{jnl}
$1s$	0.02047	0.91256	1	75.23257	$3p$	0.17486	–0.07384	2	44.51621
		0.10554	1	49.16634			0.76941	2	34.70192
		–0.07759	2	36.59489			0.00306	3	142.91730
		0.06448	2	32.00313			–0.74804	3	21.06759
		–0.01735	3	21.91011			0.26460	4	20.16670
		0.01199	3	18.74558			–0.73361	4	24.81636
		–0.00169	4	11.97154	$4p$	0.33816	0.44859	2	30.54922
		0.00088	4	8.92014			–0.92782	2	33.60156
$2s$	0.08496	0.01972	1	65.76270			–0.99885	3	21.06719
		0.57967	1	49.70330			2.23243	3	20.83745
		–0.44945	2	36.63235			77.24795	4	11.11203
		–0.85345	2	32.19828			–78.50060	4	11.19057
		0.00689	3	24.38799	$5p$	0.55857	0.76517	2	15.94698
		0.00453	3	23.07372			0.70228	2	15.77001
		0.00000	4	774.34820			2.34980	3	17.39925
		0.00536	4	90.56360			–7.83165	3	16.09765
$3s$	0.23817	–0.00346	1	81.22177			9.07239	4	15.24309
		–0.25787	1	49.16634			–5.48755	4	12.15569
		–0.42615	2	36.59261	$3d$	0.16253	–0.55012	3	23.50000
		1.25424	2	32.00392			–0.48080	3	18.84293
		0.10163	3	26.53384			0.03728	4	13.28512
		–1.66085	3	17.82918			–0.01092	4	7.42249
		2.55623	4	15.58640			0.00484	5	5.56410
		–2.32442	4	14.55794			–0.00127	5	3.69628
$4s$	0.31345	0.00169	1	83.58593	$4d$	0.33119	–2.59053	3	19.44456
		0.30979	1	48.73363			4.46604	3	19.08265
		0.56732	2	37.32465			–2.79971	4	16.67027
		–1.63220	2	31.85813			–0.15987	4	33.65818
		–1.94461	3	22.87161			–4.98899	5	17.39352
		2.59965	3	22.65146			5.59115	5	17.76746
		1.25897	4	25.31327	$5d$	0.52481	0.20406	3	27.43470
		–1.45809	4	14.37310			0.49988	3	17.88940
$5s$	0.54460	–0.00900	1	76.93152			–0.01110	4	30.18838
		0.16758	1	48.87097			0.01488	4	29.88650
		0.25279	2	38.89847			–2.47602	5	16.78989
		–0.90173	2	30.92275			2.34067	5	12.25650
		175.24223	3	11.21427	$4f$	0.27111	–0.99252	4	16.73106
		–227.08973	3	10.26120			–0.02383	4	5.83540
		–631.10285	4	11.54065	$5f$	0.50092	1.94693	4	14.90661
		687.49737	4	11.42525			–2.30768	4	11.02760
$2p$	0.07144	0.08821	2	49.81390	$5g$	0.42952	1.02078	5	12.78938
		0.90932	2	33.95499			–0.02088	5	12.05930
		0.01277	3	39.84916					
		–0.00652	3	21.97709					
		0.00357	4	21.23783					
		–0.00027	4	11.84366					

specifically designed to deal with cases where relativistic effects are important, this agreement is to be expected. More surprising is the extent of the agreement between CIV3, GRASP^0, and NIST, since CIV3 is not a fully relativistic code. The best alignment occurs for the $n = 3$ levels with somewhat higher disparities evident for the $n = 4$ and $n = 5$ states. This is due to the difference between the fully relativistic and CIV3 orbitals.

We present in Table IV the transition rates (A values) for several fine-structure $E1$ transitions in the W LXIV ion, calculated using theoretical energies. In this case, we are only able to compare the results of our CIV3 and GRASP^0 calculations, since we are unaware of other data with which to compare. Comparison of the two sets of calculations shows that for the majority of the $E1$ transitions there is generally quite good agreement; in some cases the agreement is very good. The greatest disparities occur for the $3p\,^2P^o_{1/2}$–$5s\,^2S_{1/2}$, $3p\,^2P^o_{3/2}$–$5d\,^2D_{3/2}$, and $3d\,^2D_{3/2}$–$5p\,^2P^o_{1/2}$ transitions. These large differences have been traced back to spurious CI

TABLE III. Energy levels (in Ry) relative to the $2p^6 3s\ ^2S$ ground state of W LXIV from CIV3, GRASP^0, and NIST [5].

Index	Configuration	Term	J	CIV3	NIST	GRASP^0
1	$2p^6 3s$	^2S	0.5	0.00	0.00	0.00
2	$2p^6 3p$	$^2P^o$	0.5	11.59	11.73	11.87
3			1.5	38.49	39.19	39.63
4	$2p^6 3d$	^2D	1.5	53.69	52.97	53.53
5			2.5	59.68	59.21	59.93
6	$2p^6 4s$	^2S	0.5	240.70	239.12	239.56
7	$2p^6 4p$	$^2P^o$	0.5	247.83	243.92	244.46
8			1.5	258.82	255.18	255.82
9	$2p^6 4d$	^2D	1.5	261.66	260.37	261.11
10			2.5	264.37	263.09	263.87
11	$2p^6 4f$	$^2F^o$	2.5	267.57	265.94	266.50
12			3.5	268.85	267.09	267.84
13	$2p^6 5s$	^2S	0.5	349.09		346.74
14	$2p^6 5p$	$^2P^o$	0.5	349.29		348.53
15			1.5	354.65		354.23
16	$2p^6 5d$	^2D	1.5	357.81		356.83
17			2.5	359.00	357.54	358.25
18	$2p^6 5f$	$^2F^o$	2.5	360.54	358.84	359.63
19			3.5	361.14	359.46	360.24
20	$2p^6 5g$	^2G	3.5	361.65	359.77	360.43
21			4.5	361.70	360.11	360.80

cancellations in the CIV3 calculation, arising because the CIV3 radial functions are not fully relativistic.

Table V shows the A values for $E2$ transitions, again using theoretical transition energies, from both the CIV3 and GRASP^0 calculations. One of the most noticeable things about these transitions is that the poorest agreements arise from the $n = 3$ to $n = 5$ cases, again due to the differences in the way the radial functions were obtained.

However, in order to get a more accurate indication of the differences between the CIV3 and GRASP^0 models, their respective energies were shifted to the common NIST values during the course of the collisional calculation. The dipole transition rates are calculated as

$$A = \frac{64\pi^4 e^2 a_0^2 \sigma^3}{3h} \left| \langle \gamma J M | P_q^{(1)} | \gamma' J' M' \rangle \right|^2, \tag{6}$$

where a_0 is the Bohr radius, σ is the transition energy, $P_q^{(1)}$ is the qth component of the classical dipole moment of the atom measured in units of ea_0, and $\gamma' J' M'$ and $\gamma J M$ are, respectively, the energetically higher and lower states involved. When the energy levels of either of our models are shifted to the NIST values, then the $E1$ transition rates are scaled by a factor of

$$\left(\frac{\Delta E_{\rm NIST}}{\Delta E_{model}} \right)^3, \tag{7}$$

where ΔE denotes the transition energy. The effect of this scaling on the transition rates is given in Table VI. Clearly there are some changes to the transition rates, but these changes are generally small. It is seen therefore that the main difference between the results from the CIV3 and GRASP^0 calculations arises from the different manner in which relativistic effects

TABLE IV. Comparison of A values (in s^{-1}) for $E1$ fine-structure transitions between CIV3 and GRASP^0. Numbers in square brackets represent powers of 10.

Upper level	Lower level	A value CIV3	A value GRASP^0
$3s\ ^2S_{1/2}$	$3p\ ^2P^o_{1/2}$	4.19[10]	4.52[10]
$3s\ ^2S_{1/2}$	$3p\ ^2P^o_{3/2}$	1.62[12]	1.82[12]
$3s\ ^2S_{1/2}$	$4p\ ^2P^o_{1/2}$	5.06[13]	6.20[13]
$3s\ ^2S_{1/2}$	$4p\ ^2P^o_{3/2}$	3.30[13]	3.80[13]
$3s\ ^2S_{1/2}$	$5p\ ^2P^o_{1/2}$	2.33[13]	3.33[13]
$3s\ ^2S_{1/2}$	$5p\ ^2P^o_{3/2}$	2.02[13]	2.29[13]
$3p\ ^2P^o_{1/2}$	$3d\ ^2D_{3/2}$	1.47[12]	1.49[12]
$3p\ ^2P^o_{1/2}$	$4s\ ^2S_{1/2}$	1.12[13]	1.66[13]
$3p\ ^2P^o_{1/2}$	$4d\ ^2D_{3/2}$	8.21[13]	9.14[13]
$3p\ ^2P^o_{1/2}$	$5s\ ^2S_{1/2}$	2.92[11]	7.82[12]
$3p\ ^2P^o_{1/2}$	$5d\ ^2D_{3/2}$	3.10[13]	5.11[13]
$3p\ ^2P^o_{3/2}$	$3d\ ^2D_{3/2}$	1.43[10]	1.09[10]
$3p\ ^2P^o_{3/2}$	$3d\ ^2D_{5/2}$	2.45[11]	2.12[11]
$3p\ ^2P^o_{3/2}$	$4s\ ^2S_{1/2}$	4.35[13]	4.86[13]
$3p\ ^2P^o_{3/2}$	$4d\ ^2D_{3/2}$	1.91[13]	2.07[13]
$3p\ ^2P^o_{3/2}$	$4d\ ^2D_{5/2}$	1.11[14]	1.18[14]
$3p\ ^2P^o_{3/2}$	$5s\ ^2S_{1/2}$	1.95[13]	2.20[13]
$3p\ ^2P^o_{3/2}$	$5d\ ^2D_{3/2}$	9.92[12]	1.03[13]
$3p\ ^2P^o_{3/2}$	$5d\ ^2D_{5/2}$	6.20[13]	6.09[13]
$3d\ ^2D_{3/2}$	$4p\ ^2P^o_{1/2}$	1.43[13]	1.64[13]
$3d\ ^2D_{3/2}$	$4p\ ^2P^o_{3/2}$	7.14[11]	9.18[11]
$3d\ ^2D_{3/2}$	$4f\ ^2F^o_{5/2}$	2.36[14]	2.31[14]
$3d\ ^2D_{3/2}$	$5p\ ^2P^o_{1/2}$	2.59[12]	6.70[12]
$3d\ ^2D_{3/2}$	$5p\ ^2P^o_{3/2}$	8.59[10]	3.85[11]
$3d\ ^2D_{3/2}$	$5f\ ^2F^o_{5/2}$	7.28[13]	8.09[13]
$3d\ ^2D_{5/2}$	$4p\ ^2P^o_{3/2}$	8.70[12]	9.57[12]
$3d\ ^2D_{5/2}$	$4f\ ^2F^o_{5/2}$	1.63[13]	1.58[13]
$3d\ ^2D_{5/2}$	$4f\ ^2F^o_{7/2}$	2.47[14]	2.40[14]
$3d\ ^2D_{5/2}$	$5p\ ^2P^o_{3/2}$	2.14[12]	4.00[12]
$3d\ ^2D_{5/2}$	$5f\ ^2F^o_{5/2}$	4.93[12]	5.35[12]
$3d\ ^2D_{5/2}$	$5f\ ^2F^o_{7/2}$	7.82[13]	8.27[13]

are introduced in these two models. Nevertheless, the extent of the agreement is surprisingly good for such a highly ionized ion.

Finally, Table VII shows the scaled $E2$ A values. The scaling method is the same as for the electric dipole case, except that the ratio between the energy differences seen in Eq. (7) is taken to the power of 5 instead of 3.

III. COLLISION CALCULATION

In this section we report on the results from two variants of the R-matrix codes to compute the collision strength Ω_{if} and corresponding effective collision strength Υ_{if} for all transitions among the 21 fine-structure levels of the W LXIV ion. The collision strength between an initial state i and a final state f is defined in terms of the collision cross section σ_{if} by

$$\Omega_{if} = \frac{(2J_i + 1)k_i^2}{\pi} \sigma_{if}, \tag{8}$$

TABLE V. Comparison of A values (in s^{-1}) $E2$ fine-structure transitions between CIV3 and GRASP^0. Numbers in square brackets represent powers of 10.

Upper level	Lower level	A value CIV3	A value GRASP^0
$3s\ ^2S_{1/2}$	$3d\ ^2D_{3/2}$	1.45[08]	1.47[08]
$3s\ ^2S_{1/2}$	$3d\ ^2D_{5/2}$	2.60[08]	2.71[08]
$3s\ ^2S_{1/2}$	$4d\ ^2D_{3/2}$	3.92[11]	4.36[11]
$3s\ ^2S_{1/2}$	$4d\ ^2D_{5/2}$	3.96[11]	4.33[11]
$3s\ ^2S_{1/2}$	$5d\ ^2D_{3/2}$	5.26[10]	1.92[11]
$3s\ ^2S_{1/2}$	$5d\ ^2D_{5/2}$	6.02[10]	2.01[11]
$3p\ ^2P^o_{1/2}$	$3p\ ^2P^o_{3/2}$	6.16[06]	7.52[06]
$3p\ ^2P^o_{1/2}$	$4p\ ^2P^o_{3/2}$	7.60[10]	1.10[11]
$3p\ ^2P^o_{1/2}$	$4f\ ^2F^o_{5/2}$	6.23[11]	6.39[11]
$3p\ ^2P^o_{1/2}$	$5p\ ^2P^o_{3/2}$	5.10[08]	6.63[10]
$3p\ ^2P^o_{1/2}$	$5f\ ^2F^o_{5/2}$	7.50[09]	7.12[10]
$3p\ ^2P^o_{3/2}$	$4p\ ^2P^o_{1/2}$	2.15[11]	2.10[11]
$3p\ ^2P^o_{3/2}$	$4p\ ^2P^o_{3/2}$	1.07[11]	1.04[11]
$3p\ ^2P^o_{3/2}$	$4f\ ^2F^o_{5/2}$	1.29[11]	1.30[11]
$3p\ ^2P^o_{3/2}$	$4f\ ^2F^o_{7/2}$	5.96[11]	5.98[11]
$3p\ ^2P^o_{3/2}$	$5p\ ^2P^o_{1/2}$	1.36[11]	9.91[10]
$3p\ ^2P^o_{3/2}$	$5p\ ^2P^o_{3/2}$	8.72[10]	5.66[10]
$3p\ ^2P^o_{3/2}$	$5f\ ^2F^o_{5/2}$	1.15[10]	5.76[09]
$3p\ ^2P^o_{3/2}$	$5f\ ^2F^o_{7/2}$	5.88[10]	3.11[10]
$3d\ ^2D_{3/2}$	$3d\ ^2D_{5/2}$	7.45[02]	8.71[02]
$3d\ ^2D_{3/2}$	$4s\ ^2S_{1/2}$	3.29[10]	3.76[10]
$3d\ ^2D_{3/2}$	$4d\ ^2D_{3/2}$	5.45[10]	6.09[10]
$3d\ ^2D_{3/2}$	$4d\ ^2D_{5/2}$	1.58[10]	1.73[10]
$3d\ ^2D_{3/2}$	$5s\ ^2S_{1/2}$	1.18[09]	2.08[10]
$3d\ ^2D_{3/2}$	$5d\ ^2D_{3/2}$	2.30[09]	2.85[10]
$3d\ ^2D_{3/2}$	$5d\ ^2D_{5/2}$	7.95[08]	8.44[09]
$3d\ ^2D_{3/2}$	$5g\ ^2G_{7/2}$	7.53[11]	7.16[11]
$3d\ ^2D_{5/2}$	$4s\ ^2S_{1/2}$	5.13[10]	5.47[10]
$3d\ ^2D_{5/2}$	$4d\ ^2D_{3/2}$	2.34[10]	2.51[10]
$3d\ ^2D_{5/2}$	$4d\ ^2D_{5/2}$	6.33[10]	6.71[10]
$3d\ ^2D_{5/2}$	$5s\ ^2S_{1/2}$	1.29[09]	2.98[10]
$3d\ ^2D_{5/2}$	$5d\ ^2D_{3/2}$	3.09[09]	1.13[10]
$3d\ ^2D_{5/2}$	$5d\ ^2D_{5/2}$	9.37[09]	3.16[10]
$3d\ ^2D_{5/2}$	$5g\ ^2G_{7/2}$	8.12[10]	7.91[10]
$3d\ ^2D_{5/2}$	$5g\ ^2G_{9/2}$	8.17[11]	7.83[11]

TABLE VI. Comparison of scaled A values (in s^{-1}) for $E1$ fine-structure transitions between CIV3 and GRASP^0. Numbers in square brackets represent powers of 10.

Upper level	Lower level	A value CIV3	A value GRASP^0
$3s\ ^2S_{1/2}$	$3p\ ^2P^o_{1/2}$	4.33[10]	4.36[10]
$3s\ ^2S_{1/2}$	$3p\ ^2P^o_{3/2}$	1.71[12]	1.76[12]
$3s\ ^2S_{1/2}$	$4p\ ^2P^o_{1/2}$	4.82[13]	6.18[13]
$3s\ ^2S_{1/2}$	$4p\ ^2P^o_{3/2}$	3.16[13]	3.83[13]
$3s\ ^2S_{1/2}$	$5p\ ^2P^o_{1/2}$	2.36[13]	3.40[13]
$3s\ ^2S_{1/2}$	$5p\ ^2P^o_{3/2}$	2.00[13]	2.32[13]
$3p\ ^2P^o_{1/2}$	$3d\ ^2D_{3/2}$	1.39[12]	1.44[12]
$3p\ ^2P^o_{1/2}$	$4s\ ^2S_{1/2}$	1.10[13]	1.67[13]
$3p\ ^2P^o_{1/2}$	$4d\ ^2D_{3/2}$	8.07[13]	9.14[13]
$3p\ ^2P^o_{1/2}$	$5s\ ^2S_{1/2}$	2.82[11]	8.05[12]
$3p\ ^2P^o_{1/2}$	$5d\ ^2D_{3/2}$	3.04[13]	5.12[13]
$3p\ ^2P^o_{3/2}$	$3d\ ^2D_{3/2}$	1.06[10]	1.06[10]
$3p\ ^2P^o_{3/2}$	$3d\ ^2D_{5/2}$	2.01[11]	2.03[11]
$3p\ ^2P^o_{3/2}$	$4s\ ^2S_{1/2}$	4.20[13]	4.86[13]
$3p\ ^2P^o_{3/2}$	$4d\ ^2D_{3/2}$	1.86[13]	2.05[13]
$3p\ ^2P^o_{3/2}$	$4d\ ^2D_{5/2}$	1.08[14]	1.18[14]
$3p\ ^2P^o_{3/2}$	$5s\ ^2S_{1/2}$	1.90[13]	2.24[13]
$3p\ ^2P^o_{3/2}$	$5d\ ^2D_{3/2}$	9.96[12]	1.02[13]
$3p\ ^2P^o_{3/2}$	$5d\ ^2D_{5/2}$	6.06[13]	6.15[13]
$3d\ ^2D_{3/2}$	$4p\ ^2P^o_{1/2}$	1.36[13]	1.65[13]
$3d\ ^2D_{3/2}$	$4p\ ^2P^o_{3/2}$	6.82[11]	9.32[11]
$3d\ ^2D_{3/2}$	$4f\ ^2F^o_{5/2}$	2.33[14]	2.31[14]
$3d\ ^2D_{3/2}$	$5p\ ^2P^o_{1/2}$	2.64[12]	6.94[12]
$3d\ ^2D_{3/2}$	$5p\ ^2P^o_{3/2}$	8.48[10]	3.93[11]
$3d\ ^2D_{3/2}$	$5f\ ^2F^o_{5/2}$	7.21[13]	8.10[13]
$3d\ ^2D_{5/2}$	$4p\ ^2P^o_{3/2}$	8.30[12]	9.60[12]
$3d\ ^2D_{5/2}$	$4f\ ^2F^o_{5/2}$	1.60[13]	1.57[13]
$3d\ ^2D_{5/2}$	$4f\ ^2F^o_{7/2}$	2.43[14]	2.42[14]
$3d\ ^2D_{5/2}$	$5p\ ^2P^o_{3/2}$	2.12[12]	4.00[12]
$3d\ ^2D_{5/2}$	$5f\ ^2F^o_{5/2}$	4.88[12]	5.26[12]
$3d\ ^2D_{5/2}$	$5f\ ^2F^o_{7/2}$	7.73[13]	8.36[13]

where $2J_i + 1$ is the statistical weight of the initial state and k_i^2 is the scattering channel energy. By averaging these collision strengths over a Maxwellian distribution of electron velocities, we can obtain the corresponding effective collision strength

$$\Upsilon_{if}(T_e) = \int_0^\infty \Omega_{if}(E_f) \exp\left(\frac{-E_f}{kT_e}\right) d\left(\frac{E_f}{kT_e}\right), \qquad (9)$$

where E_f is the final kinetic energy of the scattered electron, T_e is the electron temperature in degrees Kelvin, and k is Boltzmann's constant. The calculation of the effective collision strengths employs the integration methods of Burgess and Tully [16] and above the largest target state threshold the theoretical value of the collision strength was interpolated to the infinite energy limit in the manner discussed by Whiteford *et al.* [17].

Two different sets of codes were employed for the collision calculations. Initially, the Breit-Pauli RMATRXI suite [18,19], which uses the nonrelativistic orbitals from the CIV3 model discussed in the previous section, was utilized. This variant of the R-matrix codes employs LS coupling to generate the $(N + 1)$-electron matrix elements and these are then transformed to a jK coupling representation. In contrast, the Dirac atomic R-matrix code (DARC) [20] suite uses the fully relativistic orbitals from the GRASP^0 calculation and the entirety of the inner region calculations are performed relativistically. The R-matrix boundary was chosen in the former calculation to be 2.3 a.u. and in the latter to be 1.64 a.u. In both calculations the number of continuum orbitals was set to 30 and a very fine mesh (4×10^{-5} scaled Ry) of incident electron energies was employed over the entire region of interest from 0 to 1600 Ry. A finer mesh was used

TABLE VII. Comparison of scaled A values (in s^{-1}) for $E2$ fine-structure transitions from CIV3 and GRASP^0. Numbers in square brackets represent powers of 10.

Upper level	Lower level	A value CIV3	A value GRASP^0
$3s\ ^2S_{1/2}$	$3d\ ^2D_{3/2}$	1.36[08]	1.39[08]
$3s\ ^2S_{1/2}$	$3d\ ^2D_{5/2}$	2.50[08]	2.55[08]
$3s\ ^2S_{1/2}$	$4d\ ^2D_{3/2}$	3.82[11]	4.30[11]
$3s\ ^2S_{1/2}$	$4d\ ^2D_{5/2}$	3.87[11]	4.27[11]
$3s\ ^2S_{1/2}$	$5d\ ^2D_{3/2}$	5.14[10]	1.90[11]
$3s\ ^2S_{1/2}$	$5d\ ^2D_{5/2}$	5.90[10]	1.99[11]
$3p\ ^2P^o_{1/2}$	$3p\ ^2P^o_{3/2}$	6.83[06]	7.12[06]
$3p\ ^2P^o_{1/2}$	$4p\ ^2P^o_{3/2}$	7.04[10]	1.09[11]
$3p\ ^2P^o_{1/2}$	$4f\ ^2F^o_{5/2}$	6.02[11]	6.34[11]
$3p\ ^2P^o_{1/2}$	$5p\ ^2P^o_{3/2}$	5.02[08]	6.59[10]
$3p\ ^2P^o_{1/2}$	$5f\ ^2F^o_{5/2}$	7.30[09]	7.05[10]
$3p\ ^2P^o_{3/2}$	$4p\ ^2P^o_{1/2}$	1.92[11]	2.09[11]
$3p\ ^2P^o_{3/2}$	$4p\ ^2P^o_{3/2}$	9.69[10]	1.04[11]
$3p\ ^2P^o_{3/2}$	$4f\ ^2F^o_{5/2}$	1.23[11]	1.30[11]
$3p\ ^2P^o_{3/2}$	$4f\ ^2F^o_{7/2}$	5.65[11]	5.94[11]
$3p\ ^2P^o_{3/2}$	$5p\ ^2P^o_{1/2}$	1.38[11]	1.04[11]
$3p\ ^2P^o_{3/2}$	$5p\ ^2P^o_{3/2}$	8.50[10]	5.65[10]
$3p\ ^2P^o_{3/2}$	$5f\ ^2F^o_{5/2}$	1.11[10]	5.73[09]
$3p\ ^2P^o_{3/2}$	$5f\ ^2F^o_{7/2}$	5.67[10]	3.09[10]
$3d\ ^2D_{3/2}$	$3d\ ^2D_{5/2}$	9.14[02]	7.67[02]
$3d\ ^2D_{3/2}$	$4s\ ^2S_{1/2}$	3.22[10]	3.77[10]
$3d\ ^2D_{3/2}$	$4d\ ^2D_{3/2}$	5.38[10]	6.06[10]
$3d\ ^2D_{3/2}$	$4d\ ^2D_{5/2}$	1.56[10]	1.72[10]
$3d\ ^2D_{3/2}$	$5s\ ^2S_{1/2}$	1.16[09]	2.13[10]
$3d\ ^2D_{3/2}$	$5d\ ^2D_{3/2}$	2.26[09]	2.84[10]
$3d\ ^2D_{3/2}$	$5d\ ^2D_{5/2}$	7.85[08]	8.42[09]
$3d\ ^2D_{3/2}$	$5g\ ^2G_{7/2}$	7.39[11]	7.15[11]
$3d\ ^2D_{5/2}$	$4s\ ^2S_{1/2}$	4.97[10]	5.51[10]
$3d\ ^2D_{5/2}$	$4d\ ^2D_{3/2}$	2.29[10]	2.51[10]
$3d\ ^2D_{5/2}$	$4d\ ^2D_{5/2}$	6.21[10]	6.70[10]
$3d\ ^2D_{5/2}$	$5s\ ^2S_{1/2}$	1.26[09]	3.06[10]
$3d\ ^2D_{5/2}$	$5d\ ^2D_{3/2}$	3.03[09]	1.13[10]
$3d\ ^2D_{5/2}$	$5d\ ^2D_{5/2}$	9.22[09]	3.16[10]
$3d\ ^2D_{5/2}$	$5g\ ^2G_{7/2}$	7.93[10]	7.92[10]
$3d\ ^2D_{5/2}$	$5g\ ^2G_{9/2}$	8.02[11]	7.83[11]

in a separate calculation to check if convergence had been achieved in the resonance resolution and it was found that the mesh listed above was perfectly acceptable. A total of 100 000 mesh points was used in both outer region calculations. The outer region code PSTGF [18] allowed for the incorporation of the Burgess-Tully top-up method [21] to account for partial waves ranging from $2J = 80$ to infinity. The effects of radiation damping [22] were also considered, but the effects were minimal due to the high temperatures considered in our Maxwellian-averaged collision calculation. Finally, effective collisions strengths were produced for 14 temperatures ranging from 5×10^6 to 9×10^7 K, which is the region of peak abundance for this tungsten ion stage.

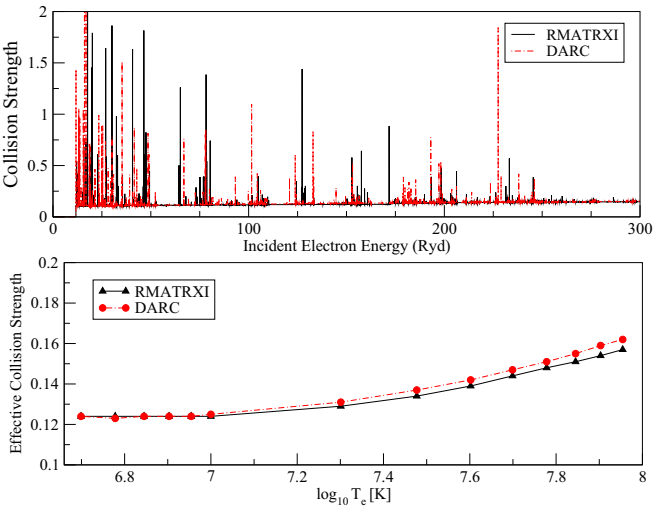

FIG. 1. Collision strengths (top) and the corresponding effective collision strengths (bottom) for the dipole-allowed $3s\ ^2S_{1/2} \rightarrow 3p\ ^2P^o_{1/2}$ (index 1-2) transition: dot-dashed lines, RMATRXI; solid lines, DARC.

Collisional atomic data

In this section collision strengths and effective collision strengths are presented for a variety of allowed and forbidden lines in W LXIV computed using the CIV3 and GRASP^0 models in the RMATRXI and DARC R-matrix suites, respectively. The results are compared in order to see the effect and suitability of adopting the different structure models for this highly ionized heavy element. While data for all 210 transitions were calculated, in this paper we present a selection of results for transitions with an initial configuration of $2p^6 3l$ ($l = s, p, d$) to emphasize our findings.

Figures 1 and 2 show the collision strengths and corresponding Maxwellian-averaged effective collision

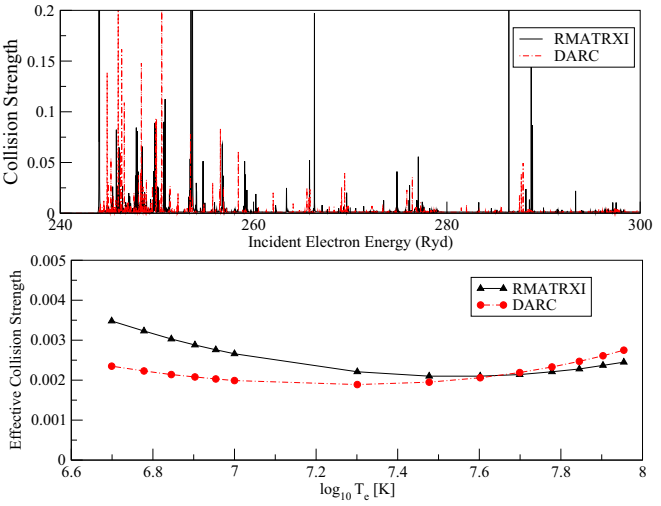

FIG. 2. Collision strengths (top) and the corresponding effective collision strengths (bottom) for the dipole-allowed $3s\ ^2S_{1/2} \rightarrow 4p\ ^2P^o_{1/2}$ (index 1-7) transition: dot-dashed lines, RMATRXI; solid lines, DARC.

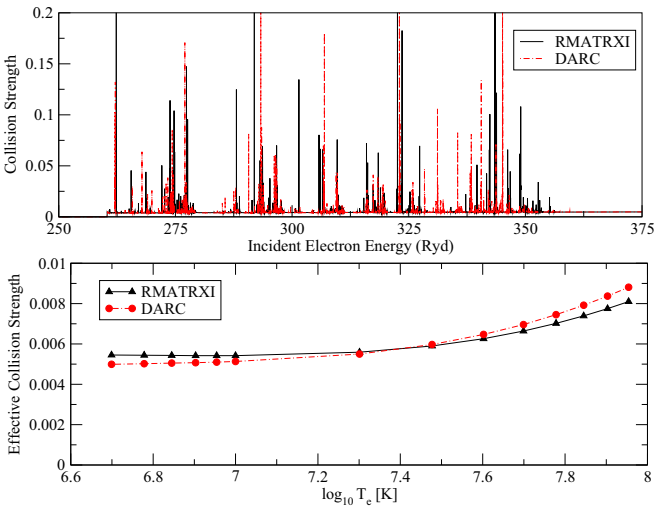

FIG. 3. Collision strengths (top) and the corresponding effective collision strengths (bottom) for the dipole-allowed $3p\,^2P^o_{1/2} \rightarrow 4d\,^2D_{3/2}$ (index 2-9) transition: dot-dashed lines, RMATRXI; solid lines, DARC.

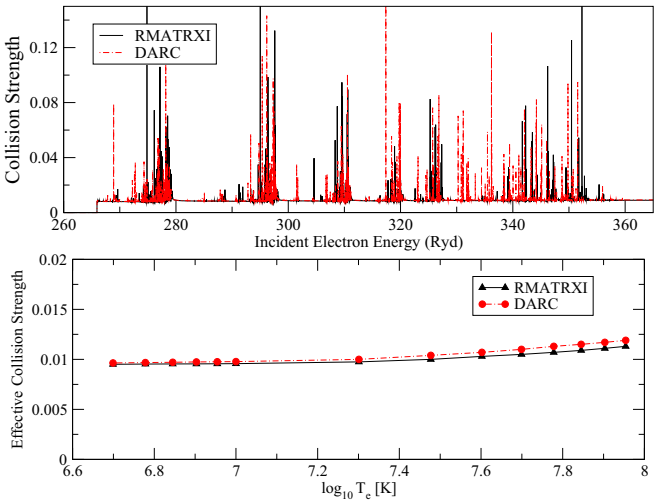

FIG. 4. Collision strengths (top) and the corresponding effective collision strengths (bottom) for the electric quadrupole $3p\,^2P^o_{1/2} \rightarrow 4f\,^2F^o_{5/2}$ (index 2-11) transition: dot-dashed lines, RMATRXI; solid lines, DARC.

strengths for two strong dipole transitions $3s\,^2S_{1/2} \rightarrow 3p\,^2P^o_{1/2}$ (index 1-2) and $3s\,^2S_{1/2} \rightarrow 4p\,^2P^o_{1/2}$ (index 1-7), respectively. Surprisingly close agreement is found for both transitions. The collision strength resonance structures coincide in regard to position and magnitude and the background cross sections show little disparity. In the top panel in Fig. 1 we see on closer analysis that the DARC results consistently lie slightly above those of the RMATRXI calculation. However, these differences, combined with some slight differences in resonance structures in the 120–160 Ry region, have only a minor effect on the corresponding effective collision strength depicted in the bottom panel. The differences amount to an average disparity of 1.37%. This is not an unsurprising result, considering the 0.69% difference in the corresponding scaled transition probability for this transition.

The $3s\,^2S_{1/2} \rightarrow 4p\,^2P^o_{1/2}$ (index 1-7) transition depicted in Fig. 2 is about 30 times weaker than the 1-2 line in Fig. 1. On careful inspection of the collision strength in the top panel we see that there are several large resonances that appear in the RMATRXI calculation that are absent in the DARC calculation. These additional features augment the corresponding effective collision strength in the low-temperature region. Despite these differences the agreement between the two calculations is on average a very acceptable 11%. The cause of these slight disparities appear to stem from the initial structure calculations. Indeed, if we look back at the relevant energy levels in Table III, we find that the CIV3 $4p$ level lies approximately 3 Ry above the value proposed by NIST or GRASP[0]. It would seem therefore that small differences in structure are significant enough to have an affect, albeit small, on the resulting collision atomic data for this ion.

In Fig. 3 we present results for another dipole-allowed transition from a metastable initial state $3p\,^2P^o_{1/2}$ to the $n = 4$ final state $4d\,^2D_{1/2}$ (index 2-9). Similar to the $3s\,^2S_{1/2} \rightarrow 4p\,^2P^o_{1/2}$ (index 2-7) case, this is a relatively weak transition. Excellent agreement, however, is evident between RMATRXI and DARC results for all incident electron energies and for all electron temperatures. On closer inspection it can be seen that the background of the DARC calculation lies very slightly below that of the RMATRXI calculation in the 250–300 Ry region and a small number of large resonances appear uniquely around the 300 and 350 Ry regions in the RMATRXI calculation. These additional features do not, however, significantly affect the corresponding Maxwellian-averaged effective collision strengths seen in the bottom panel, for which an average difference of 0.22% was recorded across the entire temperature range.

Thus far we have only considered electric dipole transitions since they represent the strongest lines for the W LXIV ion. The structure evaluations, however, revealed that there were also several strong electric quadrupole transitions with

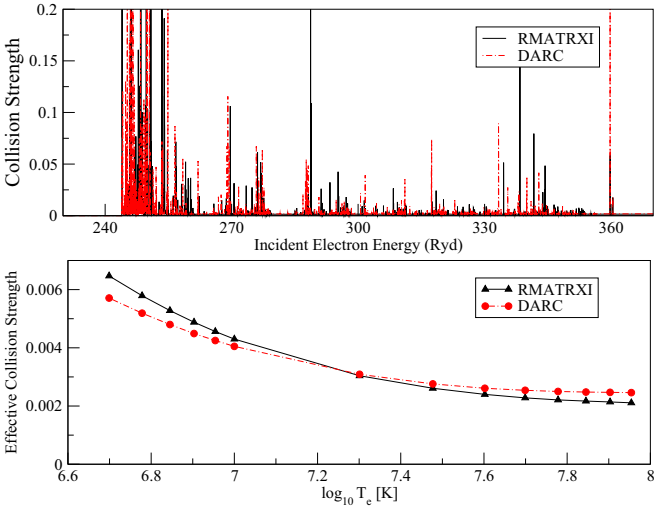

FIG. 5. Collision strengths (top) and the corresponding effective collision strengths (bottom) for the electric quadrupole $3p\,^2P^o_{3/2} \rightarrow 4p\,^2P^o_{1/2}$ (index 3-7) transition: dot-dashed lines, RMATRXI; solid lines, DARC.

A values of the order 10^{11} s^{-1}. We now consider two of these in Figs. 4 and 5, the $3p\,^2P^o_{1/2} \rightarrow 4f\,^2F^o_{5/2}$ (index 2-11) and the $3p\,^2P^o_{3/2} \rightarrow 4p\,^2P^o_{1/2}$ (index 3-7) electric quadrupole transitions. The scaled transition probabilities were calculated to be 6.02×10^{11} and 6.34×10^{11} for the CIV3 and GRASP^0 models, respectively, with a difference of 5.32%. Again, extremely good agreement is found between the collision strengths and effective collision strengths across all incident electron energies and electron temperatures. The DARC results consistently lie slightly above those of RMATRXI. The small differences in the resonance structures have little overall effect on the corresponding Maxwellian-averaged effective collisions strengths. The results differ by an average of 3.43%. A complete set of collision strengths and Maxwellian-averaged collision strengths for all 210 individual transitions are available from the authors on request.

IV. MODELING

In the context of the generalized collisional-radiative model, which properly describes the collisional regime of most astrophysical and laboratory fusion plasmas [23], excitation $\mathcal{PEC}$ associated with ion populations and spectral line emissions for the transition $j \rightarrow k$ take the form

$$\mathcal{PEC}^{(\mathrm{exc})}_{\sigma,j\rightarrow k} = A_{j\rightarrow k} F^{(\mathrm{exc})}_{j\sigma}. \tag{10}$$

Here $F^{(\mathrm{exc})}_{j\sigma}$ is the contribution to excited populations due to excitation from the metastable state σ and $A_{j\rightarrow k}$ is the A value associated with the $j \rightarrow k$ transition. Within the coronal approximation, which assumes that the only mechanism by which excited states are populated is collisional excitation and depopulation of these states only occurs by radiative decay, Eq. (10) can be rewritten as

$$\mathcal{C}_{\sigma,j\rightarrow k} = \frac{q_{\sigma\rightarrow j} A_{j\rightarrow k}}{\sum_{i<j} A_{j\rightarrow k}}, \tag{11}$$

where $q_{\sigma\rightarrow j}$ is the electron-impact excitation rate coefficient from the σth metastable state. Taking the ratio between two of these line intensities is an important tool in plasma diagnostics, as it gives vital information on the temperature or density of the plasma.

Figure 6 shows the results of calculating the photon emissivity coefficients for transitions in the W LXIV ion. It is interesting to note that while four of the five strongest intensities are from strong dipoles, the fifth is from an electric quadrupole transition from the $3d\,^2D_{3/2} \rightarrow 4s\,^2S_{1/2}$.

V. CONCLUSION

In this paper we present energy levels, A values, collision strengths, and effective collision strengths for 210 individual allowed and forbidden lines in the W LXIV ion. The radiative data were evaluated using the CIV3 and GRASP^0 structure codes, while the collisional data were computed using the RMATRXI Breit-Pauli and DARC variants of the R-matrix method. Good agreement was found when comparisons of all the atomic data were made. For the majority of the transitions considered, differences of less than 10% were recorded and for many transitions, particularly among the collisional data, the disparities were even less. This was particularly pleasing as the CIV3 structure code orbital descriptions are not fully relativistic. We would not have expected CIV3 to give results that are, in many cases, so close to those from a fully relativistic code for such a highly ionized heavy system as W LXIV.

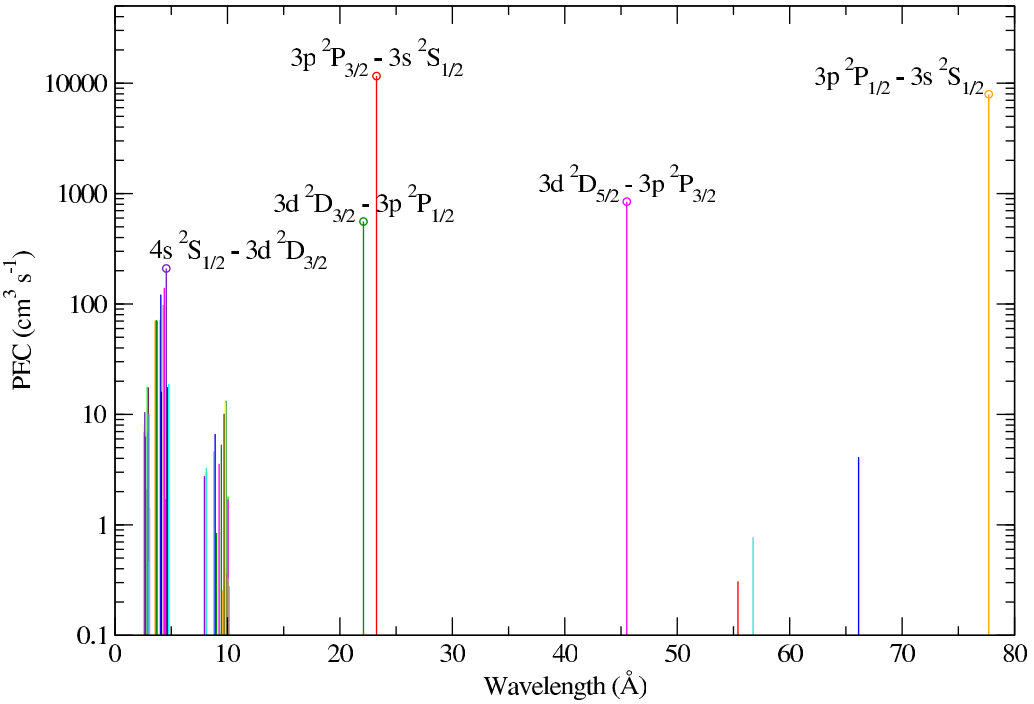

FIG. 6. Analysis of the photon emissivity coefficients on the 0–80 Å wavelength region for the W LXIV ion. The five strongest of these are annotated.

However, as we have shown, for this system carefully defined and optimized CIV3 orbital parameters can be adopted to give accurate wave-function descriptions. Spencer *et al.* [24] found that for zinclike W XLV, with two valence electrons, a similarly modified set of radial functions from CIV3 was able to give a good representation of the fully relativistic description of the ion. We would like to investigate a more complicated tungsten system in the future, one that involves several electrons outside a closed core, to verify these findings further.

ACKNOWLEDGMENTS

This work was supported by the ADAS-EU consortium and M.D.T. was funded by the Department for Employment and Learning, Northern Ireland. The computations were carried out in part on the Cray Hornet/Hazelhen supercomputer in HLRS Stuttgart under the Petascale Atomic, Molecular, Optical Physics project and partly on a local cluster funded by STFC under Grant No. L000709/1.

[1] R. A. Pitts, S. Carpentier, F. Escourbiac, T. Hirai, V. Komarov, *et al.*, J. Nucl. Mater. **438**, S48 (2013).
[2] C. P. Ballance, S. D. Loch, M. S. Pindzola, and D. C. Griffin, J. Phys. B **46**, 055202 (2013).
[3] U. I. Safranova, A. S. Safranova, and P. Beiersdorfer, At. Data Nucl. Data Tables **95**, 751 (2009).
[4] K. M. Aggarwal and F. P. Keenan, At. Data Nucl. Data Tables **100**, 1399 (2014).
[5] A. E. Kramida and T. Shirai, At. Data Nucl. Data Tables **95**, 305 (2009).
[6] Dipti, T. Das, L. Sharma, and R. Srivastava, Phys. Scr. **89**, 085403 (2014).
[7] A. Hibbert, Comput. Phys. Commun. **9**, 141 (1975).
[8] A. Hibbert, R. Glass, and C. Froese Fischer, Comput. Phys. Commun. **64**, 455 (1991).
[9] I. P. Grant, B. J. McKenzie, P. H. Norrington, D. F. Mayers, and N. C. Pypner, Comput. Phys. Commun. **21**, 207 (1980).
[10] B. J. McKenzie, I. P. Grant, and P. H. Norrington, Comput. Phys. Commun. **21**, 233 (1980).
[11] K. G. Dyall, I. Grant, C. T. Johnson, F. A. Parpia, and E. P. Plummer, Comput. Phys. Commun. **55**, 425 (1989).
[12] D. C. Griffin, N. R. Badnell, and M. S. Pindzola, J. Phys. B **31**, 3713 (1998).
[13] P. G. Burke, V. M. Burke, and K. M. Dunseath, J. Phys. B **27**, 5341 (1994).
[14] J. F. Perkins, J. Chem. Phys. **45**, 2156 (1965).
[15] A. D. McLean and R. S. McLean, At. Data Nucl. Data Tables **26**, 197 (1981).
[16] A. Burgess and J. A. Tully, Astron. Astrophys. **254**, 436 (1992).
[17] A. D. Whiteford, N. R. Badnell, C. P. Ballance, M. G. O'Mullane, H. P. Summers, and A. L. Thomas, J. Phys. B **34**, 3179 (2001).
[18] C. P. Ballance and D. C. Griffin, J. Phys. B **37**, 2943 (2004).
[19] D. M. Mitnik, D. C. Griffin, C. P. Ballance, and N. R. Badnell, J. Phys. B **36**, 717 (2003).
[20] http://connorb.freeshell.org.
[21] A. Burgess, D. G. Hummer, and J. A. Tully, Philos. Trans. R. Soc. London Ser. A **266**, 225 (1970).
[22] F. Robicheaux, T. W. Gorczyca, M. S. Pindzola, and N. R. Badnell, Phys. Rev. A **52**, 1319 (1995).
[23] H. P. Summers, N. R. Badnell, M. G. O'Mullane, A. D. Whiteford, R. Bingham, B. J. Kellett, J. Lang, K. H. Behringer, U. Fantz, K.-D. Zastrow, S. D. Loch, M. S. Pindzola, D. C. Griffin, and C. P. Ballance, Plasma Phys. Controlled Fusion **44**, B323 (2002).
[24] S. Spencer, S. Hibbert, and C. A. Ramsbottom, J. Phys. B **47**, 245001 (2014).